Crystallographic Studies on Structural Features That Determine the Enzymatic Specificity and Potency of Human Angiogenin: Thr44, Thr80, and Residues 38−41[†,‡]

Daniel E. Holloway,[§] Gayatri B. Chavali,[§,||] Michelle C. Hares,[§] Matthew D. Baker,[§] Gowtham V. Subbarao,[§] Robert Shapiro,[⊥] and K. Ravi Acharya*[,§]

Department of Biology and Biochemistry, University of Bath, Claverton Down, Bath BA2 7AY, United Kingdom, and Center for Biochemical and Biophysical Sciences and Medicine and Department of Pathology, Harvard Medical School, 77 Avenue Louis Pasteur, Boston, Massachusetts 02115

Received September 13, 2003; Revised Manuscript Received December 9, 2003

ABSTRACT: Human angiogenin (Ang) is a potent inducer of blood vessel formation and is a member of the pancreatic ribonuclease superfamily. Its enzymatic activity is unusually weak and biased toward cleavage after cytidine nucleotides. As part of an ongoing investigation into the structural basis of Ang's characteristic activity, we have determined the crystal structures of three Ang variants having novel activity. (i) The structure of T44D-Ang indicates that Asp44 can participate directly in pyrimidine binding and that the intrinsic hydrogen-bonding capability of this residue largely governs the pyrimidine specificity of this variant. Unexpectedly, the mutation also causes the most extensive disruption of the C-terminus seen in any Ang variant thus far. This allows the side chain of Arg101 to penetrate the B_1 site, raising the possibility that it participates in substrate binding as occurs in ribonuclease 4. (ii) The structure of T80A-Ang supports the view that Thr80 plays little role in maintaining the obstructive conformation of the C-terminus and that its participation in a hydrogen bond with Thr44 selectively weakens the interaction between Thr44 and N3 of cytosine. (iii) ARH-II is an angiogenin/RNase A chimera in which residues 38−41 of Ang are replaced with the corresponding residues (38−42) of RNase A. Its structure suggests that the guest segment influences catalysis by subtle means, possibly by reducing the pK_a of the catalytic lysine. The loss of angiogenic activity is not attributable to disruption of known cell-binding or nuclear translocation sites but may be a consequence of the chimera's enhanced ribonucleolytic activity.

The pancreatic ribonuclease superfamily comprises an intriguing group of biological effector proteins (*1*). Functional genes encoding eight members have been identified in the human genome (*2*), and their expression has been detected in a wide range of tissues (*2*−*5*). The best-characterized human examples are angiogenin (Ang;[1] RNase 5), an angiogenic factor involved in tumor progression (*6*); eosinophil-derived neurotoxin (EDN; RNase 2) and eosinophil cationic protein (ECP; RNase 3), two cytotoxic agents playing potential roles in innate host defense (*7*); pancreatic ribonuclease (RNase 1) (see ref *8* and references therein); and ribonuclease 4 (RNase 4) (*9*). Most of the known biological activities of these proteins are dependent on their enzymatic activity. For example, the angiogenic activity of Ang and the anti-viral properties of EDN are abolished when the proteins are rendered catalytically inactive by mutagenesis or chemical modification (*10*, *11*). It is also clear that evolutionary processes have tailored the catalytic efficiency and substrate specificity of each ribonuclease, and this may be important for the physiological roles of these enzymes.

The archetype of the pancreatic ribonuclease superfamily is bovine pancreatic ribonuclease A (RNase A; EC 3.1.27.5), an enzyme with high catalytic efficiency toward general RNA substrates (*12*, *13*). It cleaves RNA specifically after pyrimidine nucleotides without discriminating strongly between cytidine and uridine (*14*, *15*). This ambivalence is shared by EDN (*14*, *15*) and ECP (*16*) but contrasts greatly with Ang's marked (12-fold) preference for cytidine (*17*) and RNase 4's extremely strong (390-fold) preference for uridine (*18*), as measured by k_{cat}/K_m (Table 1). Thus, in moving from Ang through RNase A to RNase 4, a spectrum of pyrimidine specificity is traversed.

The nature of pyrimidine binding was first elucidated by X-ray crystallographic analyses of semisynthetic RNase A (*19*). In this enzyme, the pyrimidine-binding site (known as the B_1 subsite) is a narrow pocket formed by residues His12, Val43, Asn44, Thr45, Phe120, and Ser123. The primary

[†] This work was supported by the Wellcome Trust, U.K. (Program Grant 067288 to K.R.A.) and the National Institutes of Health (Grant CA-88738 to R.S).

[‡] The atomic coordinates of T44D-Ang, T80A-Ang, and ARH-II have been deposited in the Protein Data Bank with accession codes 1UN3, 1UN4, and 1UN5, respectively.

* To whom correspondence should be addressed. Telephone: +44-1225-386238. Fax: +44-1225-386779. E-mail: K.R.Acharya@bath.ac.uk.

[§] University of Bath.

[⊥] Harvard Medical School.

[||] Present address: Cambridge Institute of Medical Research, MRC/Wellcome Trust Building, Cambridge CB2 2XY, United Kingdom.

[1] Abbreviations: Ang, angiogenin; ARH-II, angiogenin-ribonuclease A hybrid II; ECP, eosinophil cationic protein; EDN, eosinophil-derived neurotoxin; RNase 4, ribonuclease 4; RNase A, bovine pancreatic ribonuclease A.

10.1021/bi035654+ CCC: $27.50
Published on Web 01/14/2004

Table 1: Ranking of Selected Ribonucleases on the Basis of Pyrimidine Specificity[a]

subclass	enzyme	degree of specificity $\log[(k_{cat}/K_m)_{CpA}/(k_{cat}/K_m)_{UpA}]$
cytidine-preferring	T80A-Ang	2.1[b]
	Ang	1.1[b]
	EDN	0.31[c]
	ECP	0.18[d]
	RNase A	0.15[c]
uridine-preferring	T44D-Ang	−0.48[e]
	RNase 4	−2.6[f]

[a] Enzymes are ranked by degree of specificity, from the most strongly cytidine-preferring to the most strongly uridine-preferring. Comparison is made on the basis of k_{cat}/K_m since the high (>60 mM) K_m measured between Ang and dinucleotide substrates precludes routine k_{cat} and K_m measurements on Ang variants (*29*). Values are taken from refs [b]*17*, [c]*14*, [d]*16*, [e]*26*, and [f]*18*.

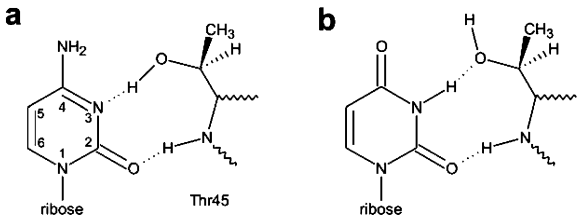

FIGURE 1: Role of Thr45 in the recognition of pyrimidines by RNase A. (a) Interaction with a cytidine nucleotide. (b) Interaction with a uridine nucleotide. Shown are those aspects of pyrimidine binding that are likely to be common to all ribonuclease superfamily members. Dotted lines denote hydrogen bonds. The atom numbering scheme common to both bases is indicated in panel (a). After Richards et al. (*19*).

functional component of this pocket is Thr45, which recognizes pyrimidines via two hydrogen bonds made with atoms in the pyrimidine ring: its main-chain NH group donates a proton to the 2-keto group of either base, and its side-chain OH group can donate to N3 of cytidine or accept from N3 of uridine (Figure 1). The importance of this residue is borne out by its conservation in the sequences of all pancreatic ribonuclease superfamily members analyzed to date.

Since the C/U specificity of these enzymes varies considerably, it is clear that residues apart from the conserved threonine must play some role in the recognition of pyrimidines. First, the properties of the conserved threonine are modulated by a neighboring, "auxiliary" residue that is remote from the substrate. For example, in RNase A, effective recognition of uridine nucleotides is dependent upon the formation of a hydrogen bond between the side chains of Thr45 and Asp83 (*20*, *21*). Second, the enzyme may make additional contacts with the pyrimidine moiety. Notable examples are the Arg101 side chain of RNase 4, which interacts directly with the 4-keto group of uridine nucleotides (*22*), and the Ser123 side chain of RNase A, which engages in two energetically significant water-mediated hydrogen bonds with the 4-keto group of uridine (*23*).

The region of Ang that corresponds to the B_1 site of RNase A contains many identical or similar elements. In Ang, residues His13, Ile42, Asn43, Thr44, Thr80, and Ile115 take the place of RNase A residues His12, Val43, Asn44, Thr45, Asp83, and Phe120, respectively (*24*, *25*). Thr44 plays a central role in pyrimidine recognition: mutations at this position have marked effects on enzymatic activity and pyrimidine specificity (*26*). In crystal structures of Ang (*24*, *25*), the Thr44 side chain engages in hydrogen bonds with the side chains of Thr80 and Gln117 (Figure 2), although the latter interaction is merely transient in solution (*27*) and is not a major determinant of the local structure (*28*). The anticipated binding position of the pyrimidine is occupied by Gln117 and Phe120. Molecular modeling and mutagenesis indicate that RNA substrates can only reasonably bind to Ang in the conventional manner, necessitating a major structural rearrangement of the C-terminal region (*28*, *29*). This partially accounts for the unusually low ribonucleolytic activity of Ang toward conventional test substrates, some 4−7 orders of magnitude lower than that of RNase A (*30*, *31*).

The basis of Ang's ribonucleolytic activity has been probed extensively by site-directed mutagenesis (see ref *25* and references therein). Although the bases of pyrimidine binding and catalysis are believed to be similar to those in RNase A, mutations at some sites have effects on pyrimidine specificity (Table 1) and/or catalytic efficiency that are not explicable by reference to the structures of Ang or RNase A. In the present report, we describe the X-ray crystal structures of three Ang mutants that fall into this category. In the first mutant, the key B_1 site residue Thr44 is replaced with Asp, converting Ang from a cytidine- to a uridine-preferring enzyme (*26*). In the second, the auxiliary residue Thr80 is replaced with Ala, increasing the enzyme's activity exclusively toward cytidine-containing nucleotides and enhancing the cleavage of polynucleotide substrates by a comparable amount (*17*). Third, we present the structure of ARH-II, an angiogenin/RNase A chimera in which residues 38−41 of Ang are replaced with the corresponding residues (38−42) of RNase A. Substitution of this segment shifts the protein's general enzymatic and angiogenic potencies toward those of RNase A (up and down, respectively) (*32*). The crystal structures give insight into the basis for the unusual kinetic properties of these variants as well as the evolution of the characteristic ribonucleolytic activity of Ang and of other members of the pancreatic ribonuclease superfamily.

EXPERIMENTAL PROCEDURES

Protein Purification, Crystallization, and Diffraction Measurements. [Pyr[1]]-T44D-Ang, [Pyr[1]]-T80A-Ang, and [Met[−1]]-ARH-II were prepared from recombinant *Escherichia coli* as described previously (*17*, *26*, *32*−*34*). This yielded proteins of >95% purity as judged by SDS−PAGE, reversed-phase HPLC, and electrospray ionization-mass spectrometry (data not shown). Crystals were grown by the hanging drop−vapor diffusion technique using conditions developed for wild-type Ang (*24*, *25*). For T44D-Ang and T80A-Ang, the reservoir consisted of 15% (w/v) PEG 4000, 0.02% (v/v) dioxane, 0.2 M sodium potassium tartrate, and 0.02 M citric acid/NaOH buffer (final pH 5.2). For ARH-II, it consisted of 10% (w/v) PEG 6000, 0.2 M sodium potassium tartrate, and 0.02 M citric acid/NaOH buffer (final pH 5.4). Drops were prepared by mixing 2 μL of protein solution (15−20 mg mL^{-1}) with 2 μL of reservoir solution and were suspended over 0.8-mL reservoirs. ARH-II crystals grew spontaneously, but to induce nucleation of the other two proteins, seeding with crystalline wild-type protein was required (*35*). In all cases, incubation at 16 °C yielded thin, platelike crystals within one week.

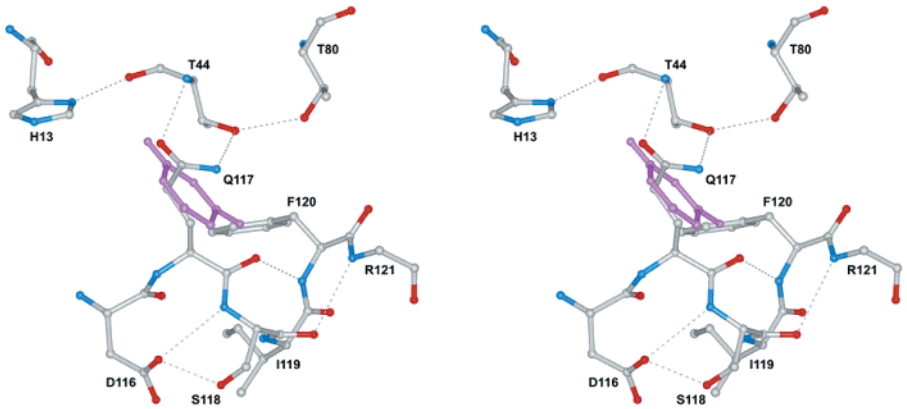

FIGURE 2: Structural context of Thr44 in angiogenin. Stereoview in which Ang (PDB entry 1B1I (*25*); CPK colors) is superposed with a uridine moiety (purple) derived from alignment of Ang with the RNase A·uridine vanadate complex (PDB entry 1RUV (*45*)). Included are Thr44, neighboring residues to which it hydrogen bonds, and residues 116−121 at the C-terminus. The side chain of Arg121 has been omitted for clarity. Dotted lines denote hydrogen bonds.

Table 2: Crystallographic Statistics

	T44D-Ang	T80A-Ang	ARH-II
	Diffraction Data		
space group	$P2_12_12$	$P2_12_12$	$C222_1$
cell dimensions (*a*, *b*, *c*) (Å)	88.4, 41.5, 33.8	86.6, 38.3, 39.0	80.3, 124.0, 37.4
resolution range (Å)	40−1.7	40−2.1	40−2.6
no. of reflections			
measured	107706	36676	35002
unique	13959	7942	5767
R_{symm}[a]	0.104 [0.377]	0.056 [0.233]	0.098 [0.257]
$I/\sigma(I)$	10.8 [9.6]	13.6 [5.1]	19.1 [8.3]
completeness (%)	97.2 [99.7]	98.6 [97.3]	95.1 [98.0]
	Final Model		
R_{cryst}[b]	0.199	0.191	0.207
R_{free}[c]	0.223	0.232	0.237
no. of atoms			
protein	884	917	923
citrate		13	13
water	78	54	9
deviations from ideality (rms)			
bond lengths (Å)	0.010	0.011	0.010
bond angles (°)	1.28	1.26	1.34
mean *B*-factor by atom type (Å^2)			
protein	21.7	27.3	51.4
citrate		45.2	77.6
water	38.2	41.6	48.1

[a] $R_{symm} = \sum_h\sum_i[|I_i(h) - \langle I(h)\rangle|/\sum_h\sum_i I_i(h)]$, where I_i is the ith measurement and $\langle I(h)\rangle$ is the weighted mean of all measurements of $I(h)$. [b] $R_{cryst} = \sum_h|F_o - F_c|/\sum_h F_o$, where F_o and F_c are the observed and calculated structure factor amplitudes of reflection h. [c] $R_{free} = R_{cryst}$ for a randomly selected 5% of the data excluded from the refinement (*60*). Square parentheses enclose data for the outermost resolution shell (1.76−1.70 Å, 2.18−2.10 Å, and 2.66−2.60 Å for T44D-Ang, T80A-Ang, and ARH-II, respectively).

All diffraction data were collected at room temperature at the Synchotron Radiation Source (Daresbury, UK). Data for T44D- and T80A-Ang were collected on station PX9.6 to 1.7 and 2.1 Å resolutions, respectively, and data for ARH-II were collected on station PX14.1 to 2.6 Å resolution. The data were indexed, scaled, and reduced using DENZO and SCALEPACK (*36*), and intensities were truncated to amplitudes using TRUNCATE (*37*). Detailed data processing statistics are given in Table 2.

Phase Determination and Refinement. Initial phases were determined by the molecular replacement method, employing the coordinates of wild-type Ang (PDB entry 1B1I for the [Pyr^1] variants; PDB entry 2ANG for the [Met^{-1}] variant) (*25*), modified appropriately at the mutation site, as a search model for AMoRe (*38*). Models produced by AMoRe were subjected to cycles of refinement in which simulated annealing, coordinate minimization, and *B*-factor refinement with CNS (*39*) were alternated with manual model building using O (*40*). During the final stages, restrained refinement and electron density map calculations were performed with REFMAC5 (*41*). Those residues with partial density were truncated accordingly, and residues for which there was no discernible density were omitted. Hydrogen-bonded water molecules were incorporated where appropriately positioned 3σ electron density was present in sigmaA-weighted $F_o - F_c$ electron density maps, and a citrate ion was incorporated into each of the T80A-Ang and ARH-II models. Detailed statistics for each model are given in Table 2.

The final T44D-Ang, T80A-Ang, and ARH-II models comprised residues 3−117, 3−121, and 3−123, respectively. Assessment of the geometry of each model with PROCHECK (*42*) confirmed that all residues had acceptable geometry and lay in the allowed regions of the Ramachandran plot.

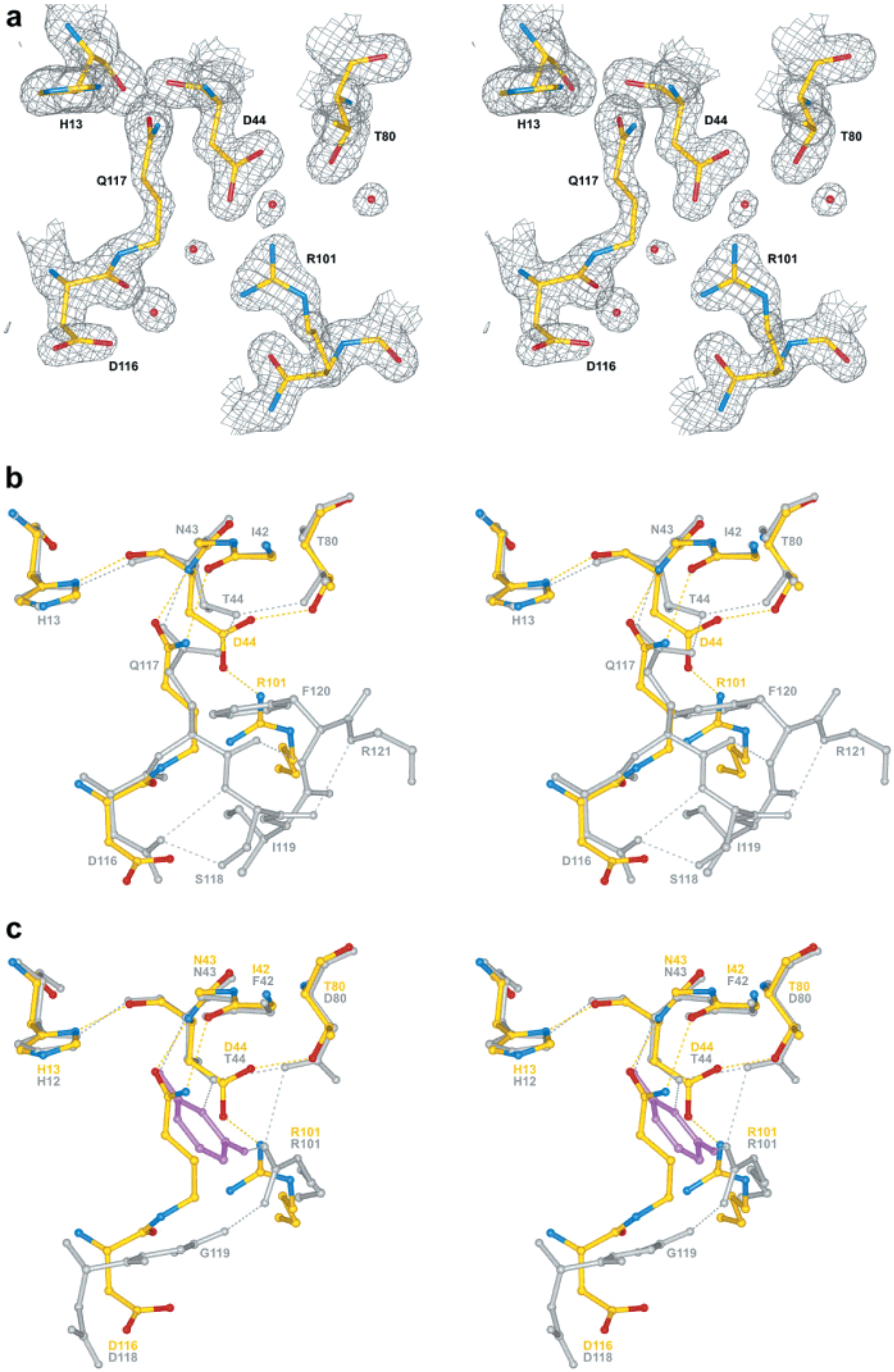

FIGURE 3: Structure of T44D-Ang and comparison with wild-type Ang and RNase 4. Throughout, the carbon, nitrogen, and oxygen atoms of T44D-Ang are shown in yellow, blue, and red, respectively, and dotted lines denote hydrogen bonds. (a) Stereoview showing the refined T44D-Ang model and sigmaA-weighted $2F_o - F_c$ electron density map (contoured at 1.7σ) in the region of mutagenesis. Spheres denote water molecules. (b) Stereoview showing a superposition of T44D-Ang and wild-type Ang (PDB entry 1B1I (*25*); gray). (c) Stereoview showing a superposition of T44D-Ang and the RNase 4·dUp complex (PDB entry 2RNF (*22*); protein atoms in gray, uridine moiety in purple).

Structural superpositions were performed with LSQMAN (*43*), topological classification was conducted with PROMOTIF2 (*44*), and figures were drawn using PyMOL (DeLano Scientific, San Carlos, CA).

RESULTS

Structure of T44D-Ang. The T44D mutation causes a significant structural change at the C-terminus of Ang: residues 118−123 are disordered to the extent that they are not discernible in the electron density map. The C^{α} atoms of residues 3−117, however, deviate only 0.45 Å (rms) from the corresponding residues of the wild-type protein (PDB entry 1B1I) (*25*), indicating that the rest of the peptide backbone is not perturbed appreciably. The side chains of Gln12, His13, Lys40, and His114 at the catalytic center show no significant changes.

Asp44 is well defined in the electron density map (Figure 3a). Although the positions of its main chain atoms closely resemble those of Thr44 in wild-type Ang, there are ~15° differences in ϕ and χ_1 that contribute to appreciable deviations between corresponding side-chain atoms (Figure 3b). Moreover, the position of the $O^{\delta 2}$ atom is incompatible

Table 3: Potential Hydrogen Bonds[a] at the Putative B_1 Site of Ang and Its T44D-, T80A-, and ARH-II Variants

	length (Å)			
bond (donor−acceptor)	Ang[b]	T44D-Ang	T80A-Ang	ARH-II[c]
His13 $N^{\delta1}$−Thr44 O	2.9	2.8	2.9	2.8
Thr44 N−Gln117 $O^{\epsilon1}$	2.9	2.8	2.8	2.8
Thr44 $O^{\gamma1}$−Thr80 $O^{\gamma1}$	2.8			2.8
Thr80 $O^{\gamma1}$−Asp44 $O^{\delta1}$		2.7		
Arg101 NH2−Asp44 $O^{\delta2}$		2.5		
Gln117 $N^{\epsilon2}$−Ile42 O		3.2		
Gln117 $N^{\epsilon2}$−Thr44 $O^{\gamma1}$	3.1			3.1
Phe120 N−Gln117 O	3.0		3.1	2.9

[a] Potential hydrogen bonds were identified with HBPLUS (*61*) and have D−H−A angles of >120°. [b] PDB entry 1B1I (*25*). [c] Residue numbers listed for ARH-II are those of the corresponding residues in wild-type Ang.

with that of Phe120 in the wild-type protein, with major consequences for the whole C-terminal segment: residues 118−123 are apparently unable to accommodate the intrusion and have disengaged from the main body of the protein, losing all conformational order. This appears to have allowed the side chain of Arg101 to switch position from the protein surface to the putative pyrimidine-binding pocket. In its new position, the guanidinium group of Arg101 occupies the space vacated by Phe120. These changes have disrupted some of the crystal packing interactions that are present in wild-type Ang crystals, including a hydrophobic cluster involving the side chains of Phe120, Ile119, and Arg101.

In crystal structures of wild-type Ang, Thr44 $O^{\gamma1}$ engages in two hydrogen bonds: one donated to Thr80 $O^{\gamma1}$ and one accepted from Gln117 $N^{\epsilon2}$ (Figure 2; Table 3). In the T44D variant, the $O^{\delta1}$ atom of Asp44 is positioned to accept a hydrogen bond from the $O^{\gamma1}$ atom of Thr80 (mimicking the Thr44 $O^{\gamma1}$−Thr80 $O^{\gamma1}$ interaction of the wild-type protein), while the $O^{\delta2}$ atom forms a salt bridge with the guanidinium group of Arg101 (Figure 3b; Table 3). The hydrogen bond between the side chains of residues 44 and 117 has been lost and replaced with an interaction between Ile42 N and Gln117 $O^{\epsilon1}$. This is coincident with a modest shift in the conformation of Gln117, although it remains in a position that is obstructive to pyrimidine binding.

To evaluate the potential contribution of Asp44 to pyrimidine binding, we aligned the structure of T44D-Ang with the structures of RNase A·uridine vanadate (PDB entry 1RUV) (*45*), RNase A·d(CpA) (PDB entry 1RPG) (*46*), and RNase 4·dUp (PDB entry 2RNF) (*22*). The position of the main-chain N atom of Asp44 aligns closely with that of the corresponding Thr residue in each of these structures (2.7−3.0 Å distant from the O2 atom of the aligned pyrimidine), suggesting that the recognition of pyrimidine 2-keto groups is likely to be preserved (Figure 3c). The β-carboxyl group of Asp44 is presumed to be essentially fully ionized under the conditions used for crystallization (pH 5.2) and assay of ribonucleolytic activity (pH 5.9−6.8) (*26*), and it is therefore likely to be an obligate hydrogen bond acceptor. As originally envisaged (*26*), a group of this type would be unable to bind cytidine nucleotides effectively but may be able to bind uridine nucleotides if positioned appropriately. The observed position of the β-carboxyl group of Asp44 is such that its $O^{\delta2}$ atom is 2.7−3.0 Å from the N3 atom of the aligned pyrimidines, but with an angle of approach that is too small to satisfy hydrogen-bonding requirements. During nucleotide binding, this might plausibly be alleviated by modest changes in the torsion angles of the Asp44 side chain, provided that these are permitted by the neighboring side chains of Thr80 and Arg101. Hence, Asp44 may participate directly in pyrimidine binding.

Structure of T80A-Ang. The polypeptide backbone of Ang is essentially unperturbed by the T80A mutation, deviating just 0.23 Å (rms) from that of the wild-type protein over all discernible C^{α} atoms (residues 3−121). At the catalytic center, the conformations of His13 and His114 are unchanged, as are the positions of the main-chain atoms of Lys40 and Gln12. The side chains of the latter two residues are partially disordered such that there is no discernible density for the N^{ζ} atom of Lys40 and there is weak density for the γ-amide group of Gln12. However, the conformational variation of these two residues among crystal structures of various ribonucleases suggests that, in the absence of substrate, they are intrinsically mobile and there is no reason to believe that the catalytic site has been perturbed significantly.

The position of Ala80 is well defined in the electron density map (Figure 4a). Its atoms occupy positions essentially the same as those of the corresponding atoms of the wild-type residue. The conformation of its neighbor, Thr44, remains unchanged, but owing to a shift in the position of Gln117, the hydrogen bond between the side chains of Thr44 and Gln117 is not present (Figure 4b; Table 3). The main chain of Thr44, however, maintains its hydrogen bond to the side chain of Gln117, and the latter residue occupies a position that is obstructive to pyrimidine binding.

Structure of ARH-II. The ARH-II chimera maintains the α/β fold common to Ang and RNase A (Figure 5b). Overall, the main chain of the protein is not perturbed greatly by the substitution (Figure 5c), deviating just 0.34 Å (rms) from the main chain of Ang (PDB entry 1B1I (*25*)) over 119 equivalent C^{α} atoms (Ang residues 3−36 and 38−122). The greatest perturbation of the host portion is seen in the loop linking strands B4 and B5. Here, the C^{α} atoms of ARH-II residues 87−90 deviate between 0.73 and 1.21 Å from their Ang counterparts (residues 86−89). This appears to be a minor adjustment required to avert potential clashes between neighboring guest (Asp38-Arg39-Cys40) and host (Pro89-Trp90) residues. However, this is not likely to have consequences for ribonucleolytic activity because Ang residues 86−89 are distant from the active site and mutations in this loop have no effect on enzymatic activity (R. Shapiro, unpublished results). The mean *B*-factor for the whole structure (51.4 $Å^2$) is slightly higher than that for the structure of [Met^{-1}]-Ang determined at 2.0 Å resolution (41.0 $Å^2$) (*25*).

Most atoms of the guest segment are well defined in the final electron density map, the exceptions being those of the Arg39 side chain beyond C^{γ}, for which no electron density is discernible, and those of the Asp38 β-carboxylate, for which there is weak density (Figure 6a). These side chains appear to protrude into the bulk solvent and are presumed to be highly mobile. The mean main-chain *B*-factor for the loop linking helix H2 with strand B1 (residues 33−42; 58.2 $Å^2$) is slightly higher than that for the whole protein, as is the case for the corresponding loops in Ang and RNase A (PDB entry 7RSA (*47*)).

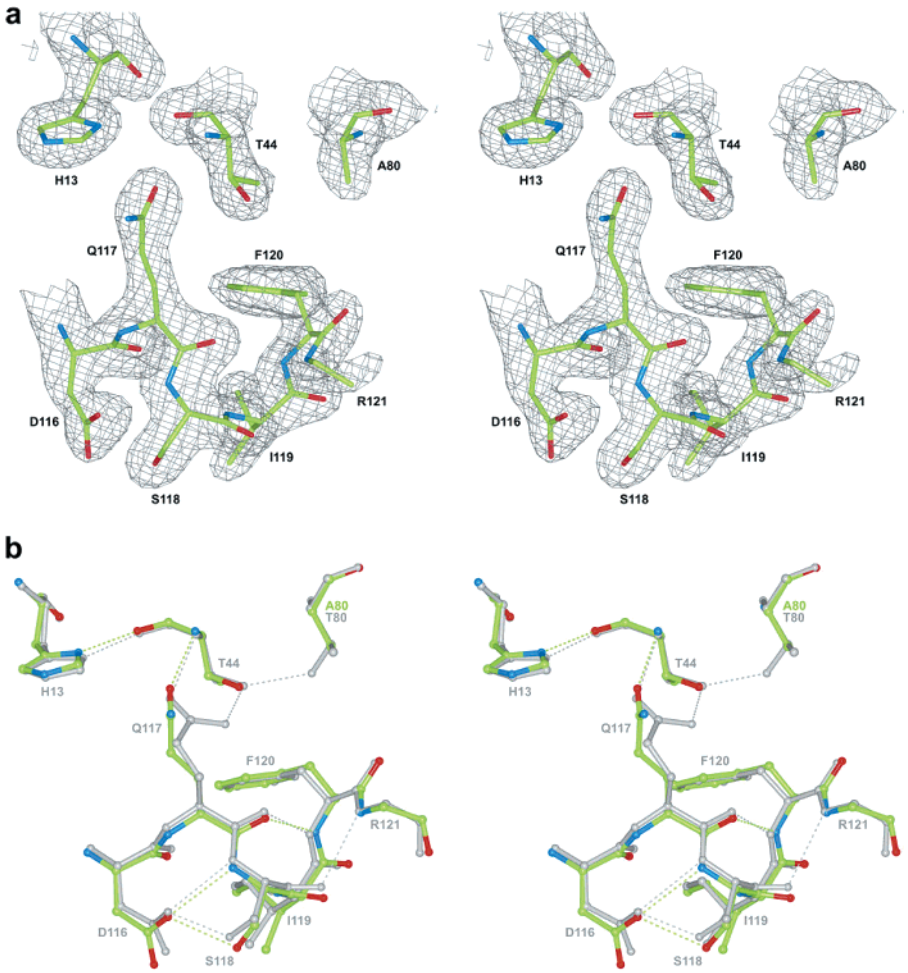

FIGURE 4: Structure of T80A-Ang and comparison with wild-type Ang in the region of mutagenesis. Throughout, the carbon, nitrogen, and oxygen atoms of T80A-Ang are shown in green, blue, and red, respectively, and dotted lines denote hydrogen bonds. (a) Stereoview showing the refined T80A-Ang model and sigmaA-weighted $2F_o - F_c$ electron density map, contoured at 1.3σ. (b) Stereoview showing a superposition of T80A-Ang and wild-type Ang (PDB entry 1B1I (*25*); gray).

Alignment of the structures of ARH-II, Ang, and RNase A, either globally or on the basis of their catalytic triad positions, allows similar conclusions to be drawn. No major perturbation of the host portion of ARH-II is observed upstream of Ser37 (Figures 5d and 6b). This residue, however, undergoes a significant positional and conformational change in order to accommodate the guest segment: its C^α atom is displaced by 3.1 Å, and its ϕ and φ angles change by +90° and −133°, respectively, closely matching those of Lys37 in RNase A (Figure 6c). The following residue, Asp38, approximates the conformation of its counterpart in RNase A and has no spatial counterpart in Ang. In addition, the 37−38 peptide bond adopts the trans conformation (as in RNase A) rather than the cis conformation seen in Ang. In this way, two residues are accommodated into this part of the loop in place of one, and the main chain is able to come back into alignment with the Ang structure immediately downstream, the C^α atoms of ARH-II Arg39 and Ang Pro38 coinciding within 0.51 Å. Although the conformations of ARH-II residues 37 and 38 resemble those of the equivalent residues in RNase A, their positions in space differ somewhat. In fact, the guest segment resembles Ang more than RNase A in the way that it is oriented relative to the main body of the protein (Figure 5d). Furthermore, residues 36−39 of ARH-II form a type IV β-turn (as in Ang) rather than the type I β-turn found in RNase A, while residues 40−43 adopt an unclassified turn (as in RNase A) rather than the type IV β-turn found in Ang. Thus, the guest segment adopts a structure that corresponds to neither RNase A nor Ang but rather is a hybrid structure.

The catalytic center and pyrimidine-binding site of ARH-II are defined clearly in the electron density map. When compared with the structure of Ang, there is no significant change in the positions/interactions of the residues at the P_1 site, i.e., those equivalent to Ang Gln12, His13, Lys40, His114, and Ile115, nor is there any change of this type among the residues that form the B_1 site, i.e., those equivalent to Ang Ile42, Asn43, Thr44, and Thr80 (Figure 6d; Table 3). In addition, the C-terminal segment, i.e., the segment equivalent to Ang positions 116−122, adopts the same obstructive conformation.

DISCUSSION

Structure−Activity Relationships of T44D-Ang. By analogy with Thr45 of RNase A, Thr44 is believed to be a key substrate-binding component of Ang. This is borne out by the substantial loss in enzymatic activity (a 25-fold drop in the rate of tRNA cleavage) that results when Thr44 is replaced with Ala (*26*). Although this mutation reduces $(k_{cat}/K_m)_{CpA}$ 24-fold, $(k_{cat}/K_m)_{UpA}$ is reduced less than 3-fold, yielding an enzyme with negligible C/U preference. This

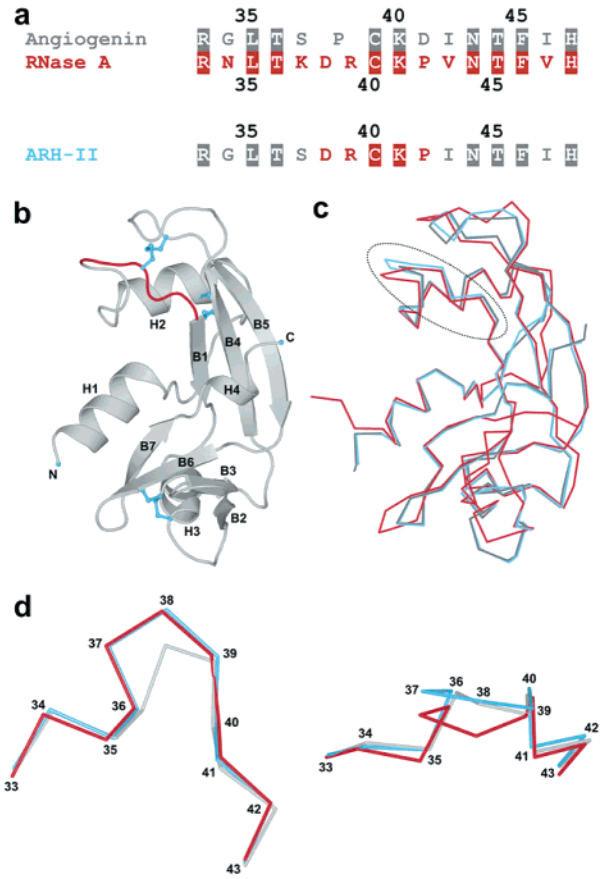

FIGURE 5: Structural overview of ARH-II. (a) Sequences of Ang (gray), RNase A (red), and ARH-II (colored according to protein of origin) in the region of mutagenesis. Residues that appear to be conserved are highlighted. (b) Schematic representation of ARH-II highlighting strands B1−B7 and helices H1−H4. The Ang-derived component is gray, the RNase-derived component is red, and disulfide bridges are light blue. (c) Global superposition of the α-carbon traces of ARH-II (light blue), Ang (PDB entry 1B1I (*25*); gray), and RNase A (PDB entry 7RSA (*47*); red), in the same orientation as in panel (b). The guest segment of ARH-II is ringed. (d) Orthogonal views of the α-carbon traces of ARH-II, Ang, and RNase A in the region of mutagenesis. The two views are related by a 90° rotation about the *x*-axis. Numbering of the ARH-II/RNase A residues is given.

suggests that a relatively stronger bond between Thr44 and N3 of cytidine nucleotides accounts for the 12-fold preference of wild-type Ang for cytidine over uridine nucleotides.

Removal of the hydrogen bond donation potential of Thr44 by replacing Thr44 with Asp causes an even more dramatic change in substrate specificity: activity toward CpN′ dinucleotides decreases 17−40-fold, while that toward UpN′ almost doubles (*26*). Consequently, T44D-Ang favors uridine over cytidine by a factor of 3−5 (Table 1). The crystal structure of T44D-Ang now indicates that direct participation of Asp44 in pyrimidine binding may account for this to some degree. In addition, a major disruption of the C-terminal segment allows the movement of the Arg101 side chain into the environs of the B_1 site, raising the possibility of the participation of this residue in substrate binding. Intriguingly, Arg101 forms part of the pyrimidine-binding site of another member of the pancreatic ribonuclease superfamily, RNase 4 (*18*, *22*, *48*). Here, the arrangement is permitted by a relatively short polypeptide chain that terminates at residue 119 (the equivalent of Gln117 in Ang). This parallels the effect of the disengagement of the C-terminus on the behavior of Arg101 in Ang and indicates that the truncation of the C-terminus was a key event in the evolution of the novel substrate specificity of RNase 4. Furthermore, when the two proteins are superposed, the guanidinium groups of their Arg101 residues overlap (Figure 3c).

In RNase 4, Arg101 plays a significant role in governing the enzyme's strong uridine specificity (*48*). The crystal structures of RNase 4 and RNase 4•dUp indicate that Arg101 impacts on pyrimidine binding in two ways (*22*). First, its guanidinium group forms a direct and specific hydrogen bond with the 4-keto group of uridine. A modest reorientation of the equivalent residue would enable the same interaction to be made in T44D-Ang, thus increasing the strength of uridine binding. Second, in RNase 4, the guanidinium group acts in concert with Phe42 (the counterpart of Ile42 in Ang) to orient the carboxylate group of Asp80, which in turn promotes Thr44's interaction with uridine (*22*, *48*, *49*). A further salt bridge between Arg101 and the nearby carboxylate group of Gly119 completes an Asp80-Arg101-Gly119 salt bridge network that appears to hold the guanidinium group firmly in position (*22*). This contrasts with the arrangement in T44D-Ang, where a Thr residue takes the place of Asp80, and there is no anionic group placed to emulate the carboxylate group of Gly119. Consequently, Arg101 is drawn toward Asp44, and it would seem that this aspect of RNase 4's uridine-binding mechanism is not in operation, offering an explanation as to why the uridine specificity of T44D-Ang is much less stringent than that of RNase 4.

The T44D-Ang structure features the most extensive disruption of the Ang C-terminus seen for any Ang variant to date. In disengaging from the main body of the protein, the two hydrogen bonds between Asp116 and Ser118 have been lost, as have the main-chain hydrogen bonds of the 3_{10}-helix. In addition, Ile119 and Phe120 are no longer buried in a hydrophobic pocket but instead are exposed to solvent. This far exceeds the scale of the perturbations seen in the structures of other Ang variants whose C-terminal residues have been mutated directly. A pertinent example is the structure of I119A/F120A-Ang, in which the mobility of the whole 117−123 segment is dramatically increased, although not by enough to bring about substantial changes in the positions of residues 117−120 (*28*). Interestingly, in this variant, the space previously occupied by the phenyl group of Phe120 is taken up partially by the guanidinium group of Arg101. However, the C-terminus remains engaged (although weakly so), preventing the guanidinium group from encroaching on the pyrimidine-binding site to the extent that it does in T44D-Ang.

It is possible that the T44D-Ang structure provides a glimpse of some of the structural rearrangements that occur upon the encounter of substrate by wild-type Ang. If this encounter induces the melting of the C-terminal segment on a comparable scale, the side chain of Arg101 might be free to participate in the recognition of the 4-keto group of uridine nucleotides as it does in RNase 4. Additional support for this proposal is provided by the kinetic properties of Ang and RNase 4 variants in which the influence of residue 80 has been removed: T80A-Ang and D80A-RNase 4 exhibit remarkably similar CpA vs UpA preferences (128- and 98-fold in favor of CpA, respectively) (*17*, *48*) and,

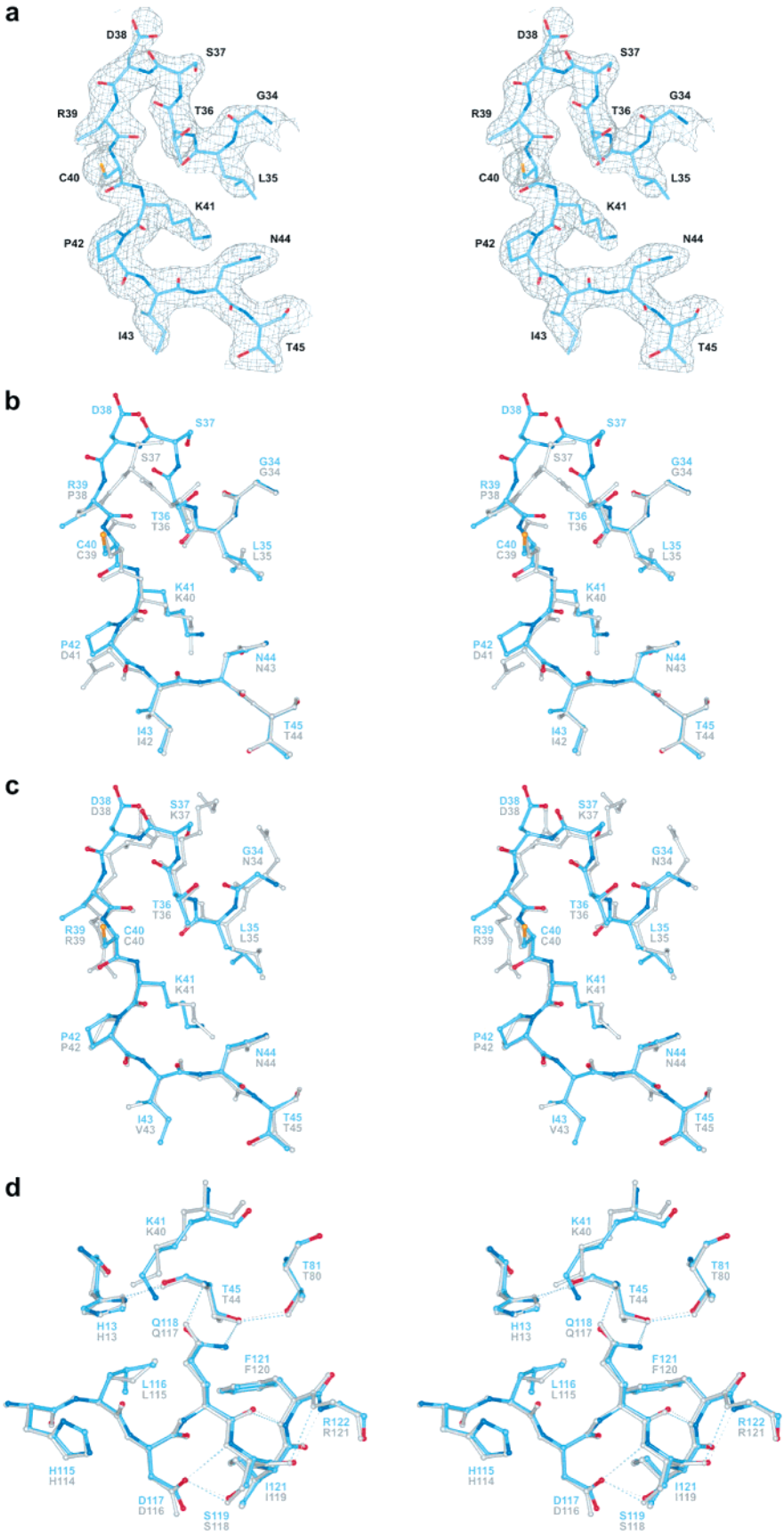

FIGURE 6: Detailed structure of the RNase A-derived guest segment in ARH-II and comparison with wild-type Ang and RNase A. Throughout, the carbon, nitrogen, and oxygen atoms of ARH-II are shown in light blue, dark blue, and red, respectively, and dotted lines denote hydrogen bonds. (a) Stereoview showing the refined ARH-II model and sigmaA-weighted $2F_o - F_c$ electron density map (contoured at 1.2σ) in the region of mutagenesis. (b) Stereoview showing a superposition of ARH-II and wild-type Ang (PDB entry 1B1I (*25*); gray) in the region of mutagenesis. (c) Stereoview showing a superposition of ARH-II and RNase A (PDB entry 7RSA (*47*); gray) in the region of mutagenesis. (d) Stereoview showing a superposition of the P_1/B_1 regions of ARH-II and wild-type Ang (PDB entry 1B1I (*25*); gray).

therefore, may have very similar modes of pyrimidine binding.

Other mutations that destabilize the conformation of the C-terminal segment have also been shown to increase the enzymatic activity of Ang several-fold (*17*, *28*, *29*, *50*−*52*). For example, I119A/F120A-Ang exhibits a 3−4-fold increase in activity toward dinucleotides and tRNA (*52*). Since the majority of the interactions holding Gln117 in its obstructive position appear to have been removed in T44D-Ang, one might have expected it to exhibit an enzymatic activity greatly above that of wild-type Ang, but this is not the case—even the enhancement of UpN′ cleavage is less than 2-fold (*26*). It seems likely that the catalytic advantage provided by the disengagement of residues 118−123 is offset by other novel structural features. One possibility is that the binding of pyrimidines to an open B_1 site containing Asp44 results in an alignment of the nucleotide with the catalytic center that is considerably less favorable than that in wild-type Ang, even for uridine nucleotides. Another is that the new Gln117-Ile42 interaction is much more stabilizing than the Gln117-Thr44 interaction is in wild-type Ang.

Structure−*Activity Relationships of T80A-Ang.* Ang possesses a Thr residue at position 80, contrasting with RNase A and RNase 4, which have an Asp at the equivalent position. In the latter two enzymes, this residue promotes the binding of uridine nucleotides through the acceptance of a hydrogen bond from the $O^{\gamma 1}$ atom of Thr45/Thr44 (*19*, *21*, *22*, *48*). In the (unliganded) Ang structure, a hydrogen bond links the $O^{\gamma 1}$ atoms of Thr44 and Thr80 (*24*, *25*) (Figure 2). This initially suggested that Thr80 might be involved in (i) suppressing the enzymatic activity of Ang by stabilizing the native, obstructive conformation of the C-terminal segment and (ii) governing Ang's 12-fold cytidine preference. The T80A mutation enhances tRNA cleavage activity 10-fold, indicating that the Thr44-Thr80 interaction indeed suppresses activity markedly (*17*). However, T80A-Ang shows an 11-fold increase in $(k_{cat}/K_m)_{CpA}$ but no change in $(k_{cat}/K_m)_{UpA}$ (resulting in a 128-fold preference for CpA), indicating that Thr80 suppresses activity primarily by attenuation of Thr44's recognition of cytidine nucleotides rather than by helping to anchor Gln117 within the B_1 site. In support of this, the K_i value for the T80A-Ang·2′-CMP interaction is reduced to half that measured with wild-type Ang (*17*). The kinetics of the Q117A- and T80A/Q117A-Ang variants confirm that Thr80's action is independent of the placement of Gln117 in the B_1 site (*17*). The importance of Thr80's role in governing the difference in pyrimidine specificity between Ang and RNase A/RNase 4 is highlighted by the change in specificity that results when Thr80 is replaced by Asp, its counterpart in the latter two enzymes: Ang's 12-fold cytidine preference is transformed into a 2-fold uridine preference, resulting chiefly from a 17-fold increase in activity toward UpA (*17*).

The structure of T80A-Ang indicates that the mutation has little effect on the stability of the C-terminal segment. Although the hydrogen bond between the side chains of Thr44 and Gln117 has been lost, the contribution that this interaction makes to the maintenance of the obstructive conformation is quite small (*27*, *28*). Moreover, the conformation of the rest of the C-terminal segment is very similar to that seen in wild-type Ang, and the hydrogen bonds that play a significant role in stabilizing it are maintained. These observations confirm the previous proposal that Thr80 plays little role in maintaining the obstructive conformation of the C-terminus (*17*).

It was proposed previously that the strong cytidine preference of T80A-Ang is attributable to the intrinsic ability of Thr44 $O^{\gamma 1}$ to form a much more effective hydrogen bond with N3 of cytidine than with that of uridine nucleotides (*17*). This implies that, in wild-type Ang, the Thr44-Thr80 hydrogen bond selectively weakens the interaction between Thr44 and N3 of cytosine. The absences of (i) new interactions involving Thr44 and (ii) significant structural perturbations in the T80A-Ang structure lend support to these views and do not necessitate the invocation of alternative explanations.

Structure−*Activity Relationships of ARH-II.* The Cys-Lys sequence motif that incorporates the active-site lysine is conserved in all pancreatic ribonuclease superfamily members studied to date. The context of the motif differs somewhat between RNase A and Ang (Figure 5a). In RNase A, an extra residue is present immediately upstream, while the Pro and Asp residues that flank the motif in Ang are transposed. Prior to the determination of the three-dimensional structure of Ang, the functional significance of these differences was probed with the aid of an angiogenin−RNase A hybrid protein, ARH-II, in which residues 38−41 of Ang are replaced with the corresponding residues (38−42) of RNase A (*32*). The protein is one of the earliest chimeric proteins generated to investigate the structural basis of functional diversity among homologous proteins. Compared to Ang, it has 5−75-fold greater enzymatic activity toward a variety of di- and polynucleotide substrates but exhibits markedly diminished angiogenic activity in vivo on the chicken embryo chorioallantoic membrane, suggesting that the residues flanking the Cys-Lys pair play a significant role in determining Ang's characteristic enzymatic activity and angiogenic potency (*32*). However, the reasons for this have been far from clear because none of the structural differences between Ang and RNase A appears to impinge directly on the catalytic center.

The structure of ARH-II now indicates that its enhanced enzymatic activity is not attributable to a major structural perturbation of Lys40 or Thr44 (Ang numbering) or any other widely recognized catalytic residue, and that the influence of the guest segment upon the catalytic apparatus is more subtle. The catalytic lysine is generally thought to stabilize the negative charge that accumulates on the nonbridging phosphoryl oxygen atoms of the RNA substrate during its cleavage, a role that relies on the donation of a hydrogen bond from its side-chain amino group to the substrate (*53*). In RNase A, the protonated form of Lys41 is destabilized by its microenvironment, depressing its pK_a to ∼9.0 (*54*). Since the strength of the hydrogen bond between the catalytic lysine and the substrate (and hence the catalytic efficiency) is expected to correlate inversely with the pK_a of the proton being donated, the pK_a shift serves to enhance catalysis (*53*). It is possible, therefore, that the change in microenvironment provided by the guest segment accounts for some of the increased enzymatic activity of ARH-II. In particular, Lys40 in Ang is adjacent to Asp41 (Figure 6b), whose carboxylate might plausibly provide some stabilization for the protonated form of Lys40 and maintain its pK_a above that of Lys41 in RNase A. Indeed, this may partially account for the generally

low enzymatic activity of Ang. In ARH-II, as in RNase A, the aspartate is transposed four residues upstream and is replaced by an apolar residue, proline. This, coupled with the positive charge of the new arginine at position 39, may be sufficient to reduce the pK_a of the catalytic lysine and thereby bring about an enhancement of catalysis in ARH-II. Such a change in pK_a might also account for the 3-fold increased rate at which the catalytic lysine is inactivated under conditions of reductive methylation (*32*).

Chemical modification of the active-site histidine residues of ARH-II occurs ~2-fold faster than in Ang (*32*), suggesting that the obligatory conformational change occurs more readily in the chimera. The guest segment does not appear to have perturbed the "closed" conformation of the enzyme, but it may have lowered the energetic barrier for the conformational switch in some other way. Thus far, it has not been possible to trap the open conformation of Ang, so the precise nature of the energetic barrier is not known. Alternatively, it is possible that the effects of this substitution become pertinent only during the transition state of the reaction.

It was suggested that ARH-II's lack of angiogenic activity might be due to an inability to bind effectively to cellular targets (*32*). The mechanism by which Ang triggers neovascularization involves its interaction with several cellular components en route from the cell surface to the nucleolus where the protein accumulates (see ref *25* and references therein). The nuclear translocation site has been shown to comprise residues 31−33 (*55*), and structural modifications of Ang that abolish cell entry but have no appreciable effect on enzymatic activity implicate residues 60−68 and Asn109 in the cell-binding process (*33*, *56*, *57*). These sites are distant from the guest segment and show no disruption in the structure of ARH-II, arguing against the presence of any deficiency in nuclear translocation or cell binding. However, the full extent of the cell-binding site has not been defined, so disruption of cell binding cannot be ruled out altogether. It seems more likely, though, that the increased enzymatic activity of ARH-II is responsible for disrupting the angiogenic response. Although the natural substrate of Ang is not known, Ang has been shown to enhance 45S rRNA synthesis in endothelial cells, suggesting that its ribonucleolytic activity is employed for the processing of pre-rRNA into ribosomes (*58*). If the enzymatic activity of Ang was any higher, it is possible that nonspecific degradation of the substrate may occur, thereby impeding the angiogenic process. In this regard, ARH-II may be a case in point.

ARH-II is the second Ang/RNase A chimera whose structure has been determined. The first was ARH-I, in which residues 58−70 of Ang are replaced with the corresponding residues (59−73) of RNase A (*31*, *59*). In contrast to the rather approximate way in which the guest segment in ARH-II resembles the parental RNase A segment, the guest segment in ARH-I adopts a structure that is highly similar to the corresponding part of RNase A. This seems likely to be because the ARH-I guest segment not only is constrained by an internal disulfide bond but also contains an element of β-structure at each end that allows integration with the β-sheet core of the host structure via main chain−main chain hydrogen bonds, promoting the adoption of its characteristic β-hairpin topology. In contrast, the ARH-II guest segment is part of an extended loop whose only strong interaction with an opposing part of the host is a disulfide bond to another flexible loop (Figure 5b). The differing fortunes of the guest segments in these two chimeras have implications for the design of novel proteins such as humanized monoclonal antibodies. They illustrate the fact that the authentic substitution of isolated loops may pose particular problems and that the chances of success may be improved by including flanking elements of higher order structure that provide additional contacts with the main body of the host.

CONCLUSIONS

The present work addresses the structural features that govern Ang's novel pyrimidine specificity and weak catalytic activity. Key findings include the following: (i) the conformational change that occurs upon substrate encounter may lead to contact between Arg101 and the substrate; (ii) the main role of Thr80 is to selectively weaken the interaction between Thr44 $O^{\gamma 1}$ and cytosine N3; and (iii) the generally low enzymatic activity of Ang may be attributable in part to maintenance of a relatively high Lys40 pK_a by the surrounding residues. Issues such as these can be resolved fully only by reference to the structure of an enzyme·substrate analogue complex. However, this has not been technically feasible because key phosphate- and purine-binding subsites in all reported Ang crystal forms are occupied by residues from neighboring symmetry-related molecules. In the absence of a complex, the properties of engineered Ang variants continue to provide valuable insight.

REFERENCES

1. D'Alessio, G., and Riordan, J. F., Eds. (1997) *Ribonucleases: Structures and Functions*, Academic Press, New York.
2. Zhang, J., Dyer, K. D., and Rosenberg, H. F. (2002) RNase 8, a novel RNase A superfamily ribonuclease expressed uniquely in placenta, *Nucleic Acids Res. 30*, 1169−1175.
3. Rosenberg, H. F., and Dyer, K. D. (1996) Molecular cloning and characterization of a novel human ribonuclease (RNase k6): increasing diversity in the enlarging ribonuclease family, *Nucleic Acids Res. 24*, 3507−3513.
4. Futami, J., Tsushima, Y., Murato, Y., Tada, H., Sasaki, J., Seno, M., and Yamada, H. (1997) Tissue-specific expression of pancreatic-type RNases and RNase inhibitor in humans, *DNA Cell Biol. 16*, 413−419.
5. Zhang, J., Dyer, K. D., and Rosenberg, H. F. (2003) Human RNase 7: a new cationic ribonuclease of the RNase A superfamily, *Nucleic Acids Res. 31*, 602−607.
6. Riordan, J. F. (1997) Structure and function of angiogenin, in *Ribonucleases: Structures and Functions* (D'Alessio, G., and Riordan, J. F., Eds.), pp 445−489, Academic Press, New York.
7. Rosenberg, H. F. (1998) The eosinophil ribonucleases, *Cell. Mol. Life Sci. 54*, 795−803.
8. Sorrentino, S. (1998) Human extracellular ribonucleases: multiplicity, molecular diversity and catalytic properties of the major RNase types, *Cell. Mol. Life Sci. 54*, 785−794.
9. Hofsteenge, J., Vicentini, A., and Zelenko, O. (1998) Ribonuclease 4, an evolutionarily highly conserved member of the superfamily, *Cell. Mol. Life Sci. 54*, 804−810.
10. Shapiro, R., and Vallee, B. L. (1989) Site-directed mutagenesis of histidine-13 and histidine-114 of human angiogenin. Alanine derivatives inhibit angiogenin-induced angiogenesis, *Biochemistry 28*, 7401−7408.
11. Domachowske, J. B., Dyer, K. D., Bonville, C. A., and Rosenberg, H. F. (1998) Recombinant human eosinophil-derived neurotoxin/RNase 2 functions as an effective antiviral agent against respiratory syncitial virus, *J. Infect. Dis. 177*, 1458−1464.
12. Richards, F. M., and Wyckoff, H. W. (1971) Bovine pancreatic ribonuclease, in *The Enzymes* (Boyer, P. D., Ed.) 3rd ed., Vol. IV, pp 647−806, Academic Press, New York.
13. Raines, R. T. (1998) Ribonuclease A, *Chem. Rev. 98*, 1045−1065.

14. Shapiro, R., and Vallee, B. L. (1991) Interaction of human placental ribonuclease with placental ribonuclease inhibitor, *Biochemistry 30*, 2246−2255.
15. Sorrentino, S., Glitz, D. G., Hamann, K. J., Loegering, D. A., Checkel, J. L., and Gleich, G. J. (1992) Eosinophil-derived neurotoxin and human liver ribonuclease. Identity of structure and linkage of neurotoxicity to nuclease activity, *J. Biol. Chem. 267*, 14859−14865.
16. Boix, E., Nikolovski, Z., Moiseyev, G. P., Rosenberg, H. F., Cuchillo, C. M., and Nogués, M. V. (1999) Kinetic and product distribution analysis of human eosinophil cationic protein indicates a subsite arrangement that favours exonuclease-type activity, *J. Biol. Chem. 274*, 15605−15614.
17. Shapiro, R. (1998) Structural features that determine the enzymatic potency and specificity of human angiogenin: threonine-80 and residues 58−70 and 116−123, *Biochemistry 37*, 6847−6856.
18. Shapiro, R., Fett, J. W., Strydom, D. J., and Vallee, B. L. (1986) Isolation and characterization of a human colon carcinoma-secreted enzyme with pancreatic ribonuclease-like activity, *Biochemistry 25*, 7255−7264.
19. Richards, F. M., Wyckoff, H. W., and Allewell, N. (1970) The origin of specificity in binding: a detailed example in a protein-nucleic acid interaction, in *The Neurosciences: Second Study Program* (Schmitt, F. O., Ed.), pp 901−912, Rockefeller University Press, New York.
20. Wlodawer, A., Miller, M., and Sjolin, L. (1983) Active site of RNase: neutron diffraction study of a complex with uridine vanadate, a transition state analog, *Proc. Natl. Acad. Sci. U.S.A. 80*, 3628−3631.
21. delCardayré, S. B., and Raines, R. T. (1995) A residue to residue hydrogen bond mediates the nucleotide specificity of ribonuclease A, *J. Mol. Biol. 252*, 328−336.
22. Terzyan, S. S., Peracaula, R., de Llorens, R., Tsushima, Y., Yamada, H., Seno, M., Gomis-Rüth, F. X., and Coll, M. (1999) The three-dimensional structure of human RNase 4, unliganded and complexed with d(Up), reveals the basis for its uridine specificity, *J. Mol. Biol. 285*, 205−214.
23. Hodges, R. S., and Merrifield, R. B. (1975) The role of serine-123 in the activity and specificity of ribonuclease. Reactivation of ribonuclease 1−118 by the synthetic COOH-terminal tetradecapeptide, ribonuclease 111−124, and its *O*-methylserine and alanine analogs, *J. Biol. Chem. 250*, 1231−1241.
24. Acharya, K. R., Shapiro, R., Allen, S. C., Riordan, J. F., and Vallee, B. L. (1994) Crystal structure of human angiogenin reveals the structural basis for its functional divergence from ribonuclease, *Proc. Natl. Acad. Sci. U.S.A. 91*, 2915−2919.
25. Leonidas, D. D., Shapiro, R., Allen, S. C., Subbarao, G. V., Veluraja, K., and Acharya, K. R. (1999) Refined crystal structures of native human angiogenin and two active site variants: implications for the unique functional properties of an enzyme involved in neovascularisation during tumour growth, *J. Mol. Biol. 285*, 1209−1233.
26. Curran, T. P., Shapiro, R., and Riordan, J. F. (1993) Alteration of the enzymatic specificity of human angiogenin by site-directed mutagenesis, *Biochemistry 32*, 2307−2313.
27. Lequin, O., Thuring, H., Robin, M., and Lallemand, J. Y. (1997) Three-dimensional solution structure of human angiogenin determined by $^{1}H,^{15}N$-NMR spectroscopy: characterization of histidine protonation states and pK_a values, *Eur. J. Biochem. 250*, 712−726.
28. Leonidas, D. D., Shapiro, R., Subbarao, G. V., Russo, A., and Acharya, K. R. (2002) Crystallographic studies on the role of the C-terminal segment of human angiogenin in defining enzymatic potency, *Biochemistry 41*, 2552−2562.
29. Russo, N., Shapiro, R., Acharya, K. R., Riordan, J. F., and Vallee, B. L. (1994) Role of glutamine-117 in the ribonucleolytic activity of human angiogenin, *Proc. Natl. Acad. Sci. U.S.A. 91*, 2920−2924.
30. Shapiro, R., Riordan, J. F., and Vallee, B. L. (1986) Characteristic ribonucleolytic activity of human angiogenin, *Biochemistry 25*, 3527−3532.
31. Harper, J. W., and Vallee, B. L. (1989) A covalent angiogenin/ribonuclease hybrid with a fourth disulfide bond generated by regional mutagenesis, *Biochemistry 28*, 1875−1884.
32. Harper, J. W., Fox, E. A., Shapiro, R., and Vallee, B. L. (1990) Mutagenesis of residues flanking Lys-40 enhances the enzymatic activity and reduces the angiogenic potency of angiogenin, *Biochemistry 29*, 7297−7302.
33. Shapiro, R., and Vallee, B. L. (1992) Identification of functional arginines in human angiogenin by site-directed mutagenesis, *Biochemistry 31*, 12477−12485.
34. Holloway, D. E., Hares, M. C., Shapiro, R., Subramanian, V., and Acharya, K. R. (2001) High-level expression of three members of the murine angiogenin family in *Escherichia coli* and purification of the recombinant proteins, *Protein Express. Purif. 22*, 307−317.
35. Stura, E. A. (1999) Seeding techinques, in *Crystallization of nucleic acids and proteins: a practical approach* (Ducruix, A., and Giegé, R., Eds.) 2nd ed., pp 177−208, Oxford University Press, Oxford.
36. Otwinowski, Z., and Minor, W. (1997) Processing of X-ray diffraction data collected in oscillation mode, *Methods Enzymol. 276*, 307−326.
37. Bailey, S. (1994) The CCP4 suite: programs for protein crystallography, *Acta Crystallogr. D50*, 760−763.
38. Navaza, J. (1994) AMoRe: an automated package for molecular replacement, *Acta Crystallogr. D50*, 157−163.
39. Brünger, A. T., Adams, P. D., Clore, G. M., DeLano, W. L., Gros, P., GrosseKunstleve, R. W., Jiang, J. S., Kuszewski, J., Nilges, M., Pannu, N. S., Read, R. J., Rice, L. M., Simonson, T., and Warren, G. L. (1998) Crystallography & NMR System: a new software suite for macromolecular structure determination, *Acta Crystallogr. D54*, 905−921.
40. Jones, T. A., Zou, J. Y., Cowan, S. W., and Kjeldgaard, M. (1991) Improved methods for binding protein models in electron density maps and the location of errors in these models, *Acta Crystallogr. A47*, 109−110.
41. Murshudov, G. N., Vagin, A. A., and Dodson, E. J. (1997) Refinement of macromolecular structures by the maximum-likelihood method, *Acta Crystallogr. D53*, 240−255.
42. Laskowski, R. A., MacArthur, M. W., Moss, D. S., and Thornton, J. M. (1993) PROCHECK: a program to check the stereochemical quality of protein structures, *J. Appl. Crystallogr. 26*, 283−291.
43. Kleywegt, G. J., and Jones, T. A. (1994) A super position, *CCP4/ESF-EACBM Newsletter on Protein Crystallography 31*, 9−14.
44. Hutchinson, E. G., and Thornton, J. M. (1996) PROMOTIF—A program to identify and analyze structural motifs in proteins, *Protein Sci. 5*, 212−220.
45. Ladner, J. E., Wladkowski, B. D., Svensson, L. A., Sjölin, L., and Gilliland, G. L. (1997) X-ray structure of a ribonuclease A-uridine vanadate compex at 1.3 Å resolution, *Acta Crystallogr. D53*, 290−301.
46. Zegers, I., Maes, D., Dao-Thi, M.-H., Poortmans, F., Palmer, R., and Wyns, L. (1994) The structures of RNase A complexed with 3′-CMP and d(CpA): active site conformation and conserved water molecules, *Protein Sci. 3*, 2322−2339.
47. Wlodawer, A., Svensson, L. A., Sjölin, L., and Gilliland, G. L. (1988) Structure of phosphate-free ribonuclease A refined at 1.26 Å, *Biochemistry 27*, 2705−2717.
48. Hofsteenge, J., Moldov, C., Vicentini, A. M., Zelenko, O., Jarai-Kote, Z., and Neumann, U. (1998) A single amino acid substitution changes ribonuclease 4 from a uridine-specific to a cytidine-specific enzyme, *Biochemistry 37*, 9250−9257.
49. Vicentini, A. M., Kote-Jarai, Z., and Hofsteenge, J. (1996) Structural determinants of the uridine-preferring specificity of RNase PL3, *Biochemistry 35*, 9128−9132.
50. Harper, J. W., and Vallee, B. L. (1988) Mutagenesis of aspartic acid-116 enhances the ribonucleolytic activity and angiogenic potency of angiogenin, *Proc. Natl. Acad. Sci. U.S.A. 85*, 7139−7143.
51. Curran, T. P., Shapiro, R., Riordan, J. F., and Vallee, B. L. (1993) Modulation of the activity of angiogenin by mutagenesis at Asp-116, *Biochim. Biophys. Acta 1202*, 281−286.
52. Russo, N., Nobile, V., Di Donato, A., Riordan, J. F., and Vallee, B. L. (1996) The C-terminal region of human angiogenin has a dual role in enzymatic activity, *Proc. Natl. Acad. Sci. U.S.A. 93*, 3243−3247.
53. Messmore, J. M., Fuchs, D. N., and Raines, R. T. (1995) Ribonuclease A: revealing structure−function relationships with semisynthesis, *J. Am. Chem. Soc. 117*, 8057−8060.
54. Jentoft, J. E., Gerken, T. A., Jentoft, N., and Dearborn, D. G. (1981) [^{13}C]Methylated ribonuclease A. ^{13}C NMR studies of the interaction of lysine 41 with active site ligands, *J. Biol. Chem. 256*, 231−236.
55. Moroianu, J., and Riordan, J. F. (1994) Identification of the nucleolar targeting signal of human angiogenin, *Biochem. Biophys. Res. Commun. 203*, 1765−1772.

56. Hallahan, T. W., Shapiro, R., and Vallee, B. L. (1991) Dual site model for the organogenic activity of angiogenin, *Proc. Natl. Acad. Sci. U.S.A. 88*, 2222−2226.
57. Hallahan, T. W., Shapiro, R., Strydom, D. J., and Vallee, B. L. (1992) Importance of asparagine-61 and asparagine-109 to the angiogenic activity of human angiogenin, *Biochemistry 31*, 8022−8029.
58. Xu, Z.-P., Tsuji, T., Riordan, J. F., and Hu, G.-F. (2002) The nuclear function of angiogenin in endothelial cells is related to rRNA production, *Biochem. Biophys. Res. Commun. 294*, 287−292.
59. Holloway, D. E., Shapiro, R., Hares, M. C., Leonidas, D. D., and Acharya, K. R. (2002) Guest−host crosstalk in an angiogenin-RNase A chimeric protein, *Biochemistry 41*, 10482−10489.
60. Brünger, A. T. (1992) The free *R*-value: a novel statistical quantity for assessing the accuracy of crystal structures, *Nature 355*, 472−474.
61. McDonald, I. K., and Thornton, J. M. (1994) Satisfying hydrogen bonding potential in proteins, *J. Mol. Biol. 238*, 777−793.

BI035654+